THE JOURNAL OF PHYSICAL CHEMISTRY B

ARTICLE

pubs.acs.org/JPCB

Aldoxime Dehydratase: Probing the Heme Environment Involved in the Synthesis of the Carbon−Nitrogen Triple Bond

Eftychia Pinakoulaki,*[,†] Constantinos Koutsoupakis,[†,∥] Hitomi Sawai,[‡] Andrea Pavlou,[†] Yasuo Kato,[§] Yasuhisa Asano,[§] and Shigetoshi Aono[‡]

[†]Department of Chemistry, University of Cyprus, P.O. Box 20537, 1678 Nicosia, Cyprus

[‡]Okazaki Institute for Integrative Bioscience, National Institutes of Natural Sciences, 5-1 Higashiyama, Myodaiji, Okazaki 444-8787, Japan

[§]Biotechnology Research Center, Faculty of Engineering, Toyama Prefectural University, 5180 Kurokawa, Imizu, Toyama 939-0398, Japan

ABSTRACT: Fourier transform infrared (FTIR) spectra, "light" minus "dark" difference FTIR spectra, and time-resolved step-scan (TRS^2) FTIR spectra are reported for carbonmonoxy aldoxime dehydratase. Two C−O modes of heme at 1945 and 1964 cm^{-1} have been identified and remained unchanged in H_2O/D_2O exchange and in the pH 5.6−8.5 range, suggesting the presence of two conformations at the active site. The observed C−O frequencies are 5 and 16 cm^{-1} lower and higher, respectively, than that obtained previously (Oinuma, K.-I.; et al. *FEBS Lett.* **2004**, *568*, 44−48). We suggest that the strength of the Fe−His bond and the neutralization of the negatively charged propionate groups modulate the ν(Fe−CO)/ν(CO) back-bonding correlation. The "light" minus "dark" difference FTIR spectra indicate that the heme propionates are in both the protonated and deprotonated forms, and the photolyzed CO becomes trapped within a ligand docking site (ν(CO) = 2138 cm^{-1}). The TRS^2-FTIR spectra show that the rate of recombination of CO to the heme is $k_{1945\ cm^{-1}} = 126 \pm 20\ s^{-1}$ and $k_{1964\ cm^{-1}} = 122 \pm 20\ s^{-1}$ at pH 5.6, and $k_{1945\ cm^{-1}} = 148 \pm 30\ s^{-1}$ and $k_{1964\ cm^{-1}} = 158 \pm 32\ s^{-1}$ at pH 8.5. The rate of decay of the heme propionate vibrations is on a time scale coincident with the rate of rebinding, suggesting that there is a coupling between ligation dynamics in the distal heme environment and the environment sensed by the heme propionates. The implications of these results with respect to the proximal His−Fe heme environment including the propionates and the positively charged or proton-donating residues in the distal pocket which are crucial for the synthesis of nitriles are discussed.

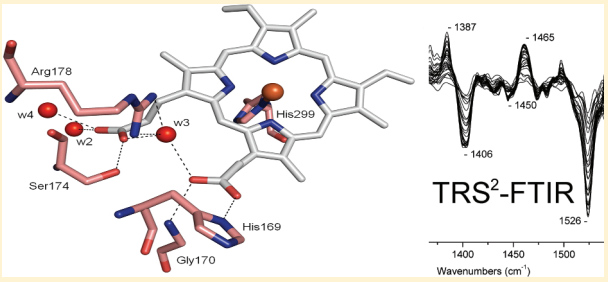

INTRODUCTION

Aldoxime dehydratase (Oxd) is a nitrile synthesizing enzyme responsible for the creation of a carbon−nitrogen triple bond and dehydration of aldoxime substrates [R—CH═N—OH] despite the presence of H_2O in the active heme Fe site.[1−11] The dehydration reaction proceeds via the N-coordinated substrate in the ferrous heme.[7,9−11] Aldoxime is coordinated to the heme Fe^{3+} through the oxygen atom, and upon reduction (heme Fe^{2+}) the aldoxime is coordinated to the heme Fe^{2+} through the nitrogen atom and subsequently converted to nitrile.[9−11] The substrate-bound ferric complex is inactive, forming a dead-end complex with the substrate.[9] The Oxd reaction is a rare example of a heme Fe directly activating an organic substrate. Therefore, it is essential to understand its function in catalyzing various aryl and alkyl aldoximes to their corresponding nitriles.

Recently, the crystal structures of the substrate-free and substrate-bound forms of Oxd from *Rhodococcus* sp. N-771 (OxdRE) were reported.[11] OxdRE forms a homodimer with each monomer containing one heme molecule. A large cavity exists on the distal environment of the heme Fe containing a H-bond network among residues Gln221, Ser219, His320, Glu143, and Arg178. Upon reduction of the protein in the presence of the substrate the hydrogen bond network is not disturbed among Glu143, Arg178, and His320 and the OH group of the heme-bound substrate forms two hydrogen bonds with His320 and Ser219. Among the determined structures significant conformational changes were observed at the proximal environment of the heme, while no conformational changes were observed at the distal environment of the heme.

The carbonmonoxy derivative of heme proteins is an extremely useful probe for studying the environment of the heme proximity. With resonance Raman spectroscopy, the frequencies of the Fe−CO and C−O stretching modes and the Fe−C−O bending modes which are particularly sensitive to the interactions with the distal environment can be measured.[12−17] Recently, it was shown that the distal environment of Oxd from *Pseudomonas chlororaphis* B23 (OxdA) possesses a single conformation at neutral pH, as judged from the single Fe−CO and CO stretching modes in the resonance Raman spectra.[5,6] OxdA has been shown to possess a distinct Fe−CO mode at 512 cm^{-1}, and the corresponding bending and C−O modes at 579 and 1950 cm^{-1}, respectively.[6] In addition, the band at 226 cm^{-1} was assigned to the Fe−His299 stretching mode.[5,6] It was concluded

Received: June 24, 2011
Revised: September 23, 2011
Published: September 26, 2011

that OxdA exhibits a relatively high Fe−His mode compared with other heme proteins containing an imidazole axial ligand, and thus a weak Fe−CO and a strong C−O mode were expected. However, the observed Fe−CO at 512 cm^{-1} and C−O at 1950 cm^{-1} are both higher, respectively, than those of many heme proteins which have a weaker Fe−His bond, including myoglobin (ν(Fe−CO) = 507 cm^{-1}).[17] To account for the observed unique spectroscopic properties of the enzyme, it was suggested that there are positively charged or proton-donating residues in the distal pocket.[6]

The investigation of pH-dependent conformational changes in the catalytic site of Oxd is a step toward the identification of groups that may be operational in the dehydration of aldoxime. Therefore, it is important to elucidate the ligand dynamics in the distal site where information is limited. In this paper, we have investigated the CO-bound OxdRE complex as a function of pH at room temperature by Fourier transform infrared (FTIR), "light" minus "dark", and time-resolved step-scan (TRS^2) FTIR spectroscopies to probe the structure of the active site and the coupled protein structural changes in response to the photodissociation/recombination of CO.

EXPERIMENTAL METHODS

Aldoxime dehydratase from *Rhodococcus* sp. N-771 was expressed and purified according to previously published procedures.[11] The samples used for the FTIR measurements had an enzyme concentration of ∼1.5 mM in 50 mM MOPS for pH 6.8 and pD 6.8, Tris for pH 8.5, and citrate for pH 5.6. The pD solutions prepared in D_2O buffers were measured by using a pH meter and assuming pD = pH (observed) + 0.4. Dithionite reduced samples were exposed to 1 atm of CO in an anaerobic cell to prepare the carbonmonoxy adduct and transferred to a tightly sealed FTIR cell with two CaF_2 windows, under anaerobic conditions (l = 15 μm). Myoglobin (Mb) from equine skeletal muscle was purchased from Aldrich and placed in 50 mM Hepes buffer (pH 7.5). CO gas was obtained from Linde. The static FTIR spectra were recorded with 4 cm^{-1} spectral resolution on a Bruker Vertex 70 FTIR spectrometer equipped with a liquid nitrogen cooled mercury cadmium telluride (MCT) detector. A 447 nm continuous wave (cw) laser diode (Coherent, Cube 445) was used as a pump beam to photolyze the CO from the OxdRE−CO adduct. The incident power on the sample was 15 mW, and 40−70 difference (light minus dark) spectra of 100 scans each were recorded and averaged.

For the time-resolved step-scan FTIR measurements, the 532 nm pulses from a Continuum Minilite II Nd:YAG laser (5 ns width, 10 Hz) were used as a pump light (8 mJ/pulse) to photolyze the OxdRE−CO adducts. These measurements were performed on a Bruker Vertex 80 V spectrometer equipped with the step-scan option. A vacuum pump was used to evacuate the interferometer compartment to a final pressure of 2.3 mbar. The FTIR spectrometer was placed on a Newport VH optical vibration isolation table to ensure that vibrational background noise from environmental sources was avoided. For the time-resolved experiments, a TTL (transistor transistor logic) pulse provided by a digital delay pulse generator (Quantum Composers, 9524) triggered flashlamps, the Q-switch, and the FTIR spectrometer. Pretriggering the FTIR spectrometer to begin data collection before the laser fires allows fixed reference points to be collected at each mirror position, which are used as the reference spectrum in the calculation of the difference spectra. Changes in intensity were recorded with a photovoltaic MCT detector

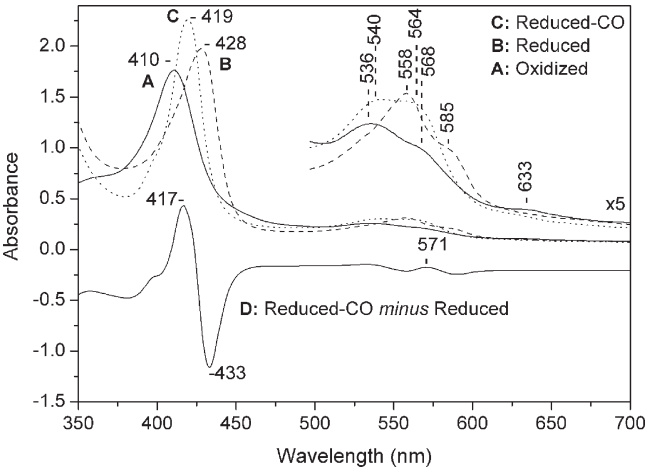

Figure 1. Optical absorption spectra of OxdRE at pH 6.8. Trace A (solid line) is the oxidized form, trace B (dashed line) is the dithionite-reduced form, and trace C (dotted line) is the reduced CO-bound form. The difference spectrum, trace D (solid line), of the reduced-CO form minus the reduced form indicates the binding of CO to the heme of OxdRE. The enzyme concentration was 7 μM, and the path length was 1 cm.

(Kolmar Technologies KV100-1B-7/190, response limit 850 cm^{-1}) and digitized with a 84-kHz, 24-bit, analog-to-digital converter (ADC). A broadband interference optical filter (LP-4200, Spectrogon) with a short wavelength cutoff at 4.2 μm was used to limit the free spectral range from 4.2 to 11.8 μm. This led to a spectral range of 2633 cm^{-1}, which was equal to an undersampling ratio of 6. Single-sided spectra were collected at 4 cm^{-1} spectral resolution, 12.5 μs time resolution, and 10 coadditions per data point. The total accumulation time for each measurement was 20 min, and five measurements were collected and averaged. Blackman−Harris three-term apodization with 32 cm^{-1} phase resolution and the Mertz phase correction algorithm were used. Difference spectra were calculated as $\Delta A = -\log(I_S/I_R)$. Optical absorption spectra were recorded with a Shimadzu UV1700 UV−visible spectrometer before and after the FTIR measurements to ensure the formation and stability of the CO adducts.

RESULTS

The optical absorption spectrum of oxidized OxdRE displays Soret maxima at 410 nm and visible bands at 536 and 568 nm and a shoulder at 633 nm which is typical of a porphyrin-to-Fe(III) charge transfer (CT) transition characteristic of ferric high spin heme *b* (Figure 1, trace A). The dithionite reduced enzyme displays Soret maxima at 428 nm and visible maxima at 558 and 585 nm (Figure 1, trace B). Carbon monoxide coordinates to the heme proteins in the reduced oxidation state, yielding characteristic spectra. Upon exposure of the reduced enzyme to an atmosphere of CO gas, a spectrum with a Soret maximum at 419 nm and visible bands at 540 and 564 nm is obtained (Figure 1, trace C). The difference spectrum of the reduced-CO form minus the reduced form is characteristic of CO binding to the heme, as denoted by the peaks at 417 and 571 nm (Figure 1, trace D).

In Figure 2 (traces A−E) we present the FTIR spectra of the CO-bound OxdRE complex at pH 5.6−8.5 and pD 6.8 at room temperature. For comparison, we have included the FTIR spectrum of Mb at pH 7.5 (Figure 2, trace F). The spectra of the CO-bound forms of OxdRE exhibit two peaks at 1945 and 1964 cm^{-1}, and their frequencies remained unchanged in the pH 5.6−8.5 range and

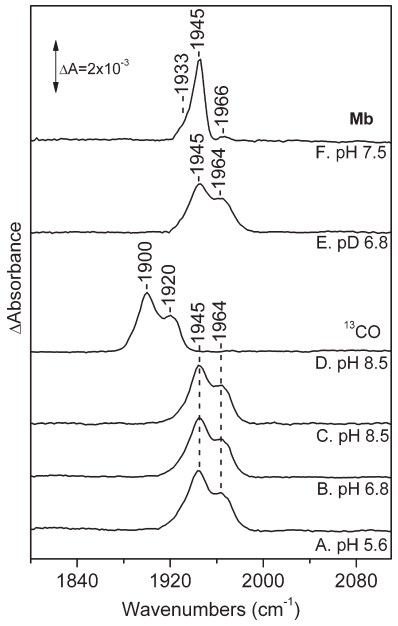

Figure 2. FTIR spectra of the OxdRE−CO adduct at pH 5.6 (trace A), pH 6.8 (trace B), pH 8.5 (trace C), and at pD 6.8 (trace E). Trace D is the spectrum of the OxdRE−^{13}CO adduct at pH 8.5. The FTIR spectrum of myoglobin−CO at pH 7.5 is included (trace F). The enzyme concentration was 1.5 mM, and the path length was 15 μm. The spectral resolution was 4 cm^{-1}.

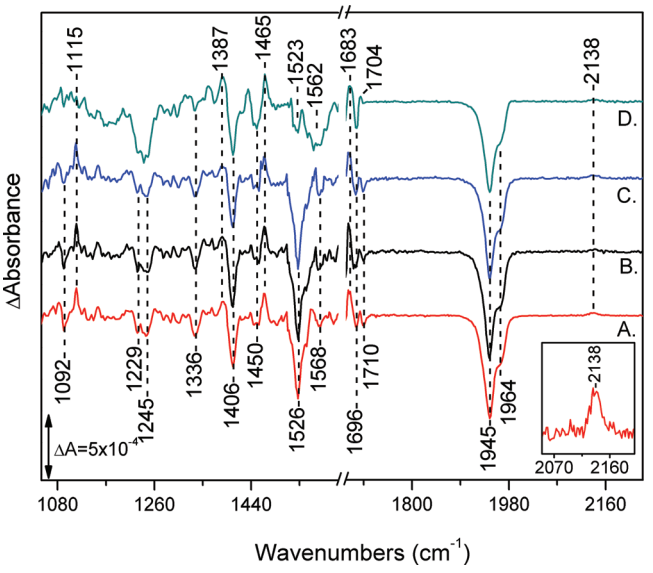

Figure 3. Light minus dark FTIR difference spectra of the OxdRE−CO adduct at pH 5.6 (trace A), pH 6.8 (trace B), pH 8.5 (trace C), and pD 6.8 (trace D). The inset shows an enlarged view of the 2138 cm^{-1} band of trace A. The enzyme concentration was 1.5 mM, and the path length was 15 μm. The spectral resolution was 4 cm^{-1}. The photolysis wavelength was 447 nm and the power incident at the sample was 15 mW.

between H_2O (Figure 2, traces A−C) and D_2O (Figure 2, trace E). The CO sensitivity of the modes is confirmed in the ^{13}CO spectrum (Figure 2, trace D), where the peaks are observed at 1900 and 1920 cm^{-1}. The spectrum of Mb−CO exhibits the major peak at 1945 (A_1 form) and two minors at 1966 (A_0 form) and 1933 cm^{-1} (A_3 form).

In the oxidized minus reduced (electrochemical) FTIR difference spectra of heme proteins, the observation of a trough/peak pattern in the 1700 cm^{-1} region (C═O of protonated carboxylic acids) has been interpreted as an environmental change induced by the change in the redox state of the metal center.[18−20] In the FTIR difference spectra obtained upon CO photolysis from the heme Fe, the appearance of a negative peak in the 1700 cm^{-1} region has been interpreted as deprotonation of a carboxyl group.[21−25] Signals in the amide I region (1620−1690 cm^{-1}) can be attributed to changes of the C═O modes caused by perturbation in the polypeptide backbone and to the C═O modes of Asn and Gln. Coupled CN stretching and NH bending modes and the asymmetric COO^- modes from deprotonated heme propionates and Glu and Asp side chains are expected in the 1530−1590 cm^{-1} region.[18−25] It has been established that the deprotonated symmetric COO^- vibrations of heme propionates and Asp residues are expected at 1350 and 1450 cm^{-1}, respectively.[18−25] In an effort to elucidate the effect of pH on the protein environment, we have investigated the light minus dark difference FTIR spectra of the CO-bound OxdRE in the pH 5.6−8.5 range (Figure 3, traces A−C) and at pD 6.8 (Figure 3, trace D). The negative peaks at 1945 and 1964 cm^{-1} indicate that both conformers are photolabile, and the positive peak at 2138 cm^{-1} demonstrates that a fraction of the photolyzed CO is funneled in a docking site of the protein.[26] We tentatively attribute the negative peaks at 1696 and 1710 cm^{-1} depicted in traces A−C to the protonated heme propionate(s) that are perturbed upon CO photolysis. The absence of the 1710 cm^{-1} trough in the pD 6.8 spectrum supports the sensitivity of the 1710 cm^{-1} mode to H/D exchange. The positive peak at 1683 cm^{-1} might be partially attributed to heme propionates because it is also the spectral region for the amide I absorbance. The 1650 cm^{-1} region that is dominated by amide I is omitted because of saturation from H_2O absorption. The negative peak at 1568 cm^{-1} shows pD sensitivity by downshifting to 1562 cm^{-1} and has contributions from the $\nu(COO^-)^{asym}$ of propionates and a Glu residue. The negative peak at 1526 cm^{-1} in the pH 5.6−8.5 range can be tentatively assigned to $\nu(COO^-)^{asym}$ of the heme propionate(s). Comparison of the pH/pD spectra shows that there is a noticeable intensity decrease and downshift by 3 cm^{-1} of $\nu(COO^-)^{asym}$ of propionates from 1526 to 1523 cm^{-1} at pD 6.8. These observations indicate that the deprotonated forms of the propionates are H-bonded with the H_2O molecule found in the crystal structure between the heme propionates.[11] Intensity changes and/or frequency shifts of the symmetric and asymmetric vibrations that could be attributed to both the deprotonated forms of heme propionates and Glu are observed in Figure 3. These include the peak/trough at 1387/1406 ($\nu(COO^-)^{sym}$) of heme propionates and the peak/trough at 1465/1450 cm^{-1} ($\nu(COO^-)^{sym}$) of Glu. The appearance of COO(H) modes ascribed to both protonated and deprotonated heme propionates in the difference FTIR spectra indicates the presence of both conformations.

Figure 4A shows the step-scan time-resolved FTIR difference spectra (t_d = 12.5 μs−15 ms, 4 cm^{-1} spectral resolution) of fully reduced OxdRE-CO subsequent to CO photolysis by a 532 nm nanosecond laser at 10 Hz. Under our experimental conditions (4 cm^{-1} spectral resolution) the 1945 and 1964 cm^{-1} peaks are well resolved, and thus we can monitor their individual kinetic behavior. The negative peaks at 1945 and 1964 cm^{-1} arise from the photolyzed heme Fe−CO. No significant intensity variations are detected in the transient difference spectra (t_d = 12−300 μs)

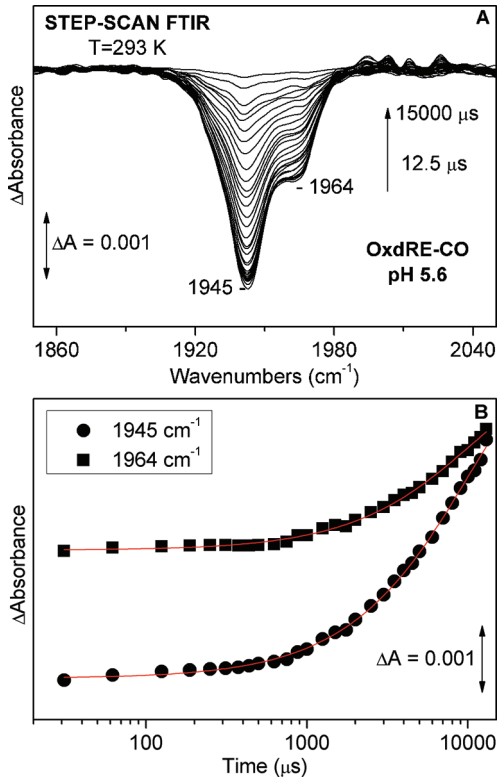

Figure 4. (A) Time-resolved step-scan FTIR difference spectra of the OxdRE−CO adduct at pH 5.6 at 0.012, 0.037, 0.062, 0.125, 0.187, 0.250, 0.312, 0.375, 0.437, 0.500, 0.625, 0.750, 0.875, 1, 1.25, 1.5, 1.75, 2, 2.5, 3, 3.5, 4, 4.5, 5, 6, 7, 8, 9, 10, 11, 12, 13, and 15 ms subsequent to CO photolysis. (B) Plot of the ΔA of the 1945 (circles) and 1964 cm^{-1} (squares) modes versus time on a logarithmic scale subsequent to CO photolysis. The red lines correspond to the exponential fit of the experimental data.

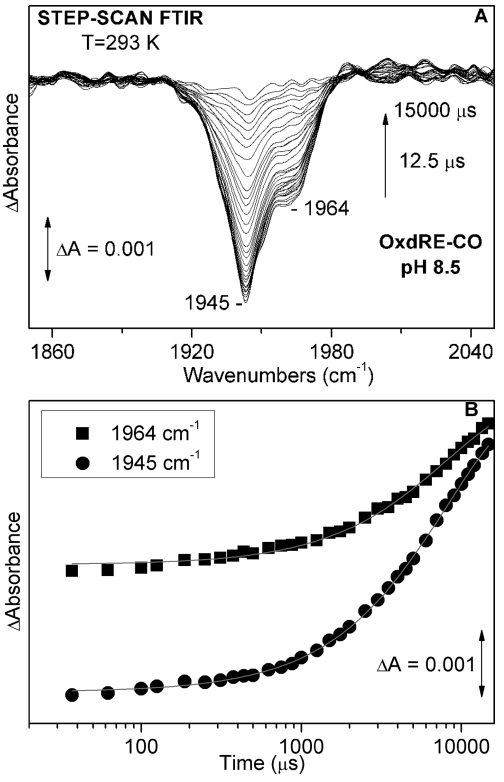

Figure 5. (A) Time-resolved step-scan FTIR difference spectra of the OxdRE−CO adduct at pH 8.5 at 0.012, 0.037, 0.062, 0.125, 0.187, 0.250, 0.312, 0.375, 0.437, 0.500, 0.625, 0.750, 0.875, 1, 1.25, 1.5, 1.75, 2, 2.5, 3, 3.5, 4, 4.5, 5, 6, 7, 8, 9, 10, 11, 12, 13, and 15 ms subsequent to CO photolysis. (B) Plot of the ΔA of the 1945 (circles) and 1964 cm^{-1} (squares) modes versus time on a logarithmic scale subsequent to CO photolysis. The red lines correspond to the exponential fit of the experimental data.

for either of the 1945 and 1964 cm^{-1} modes. At later times, however, a decreasing intensity is observed, suggesting the onset of CO rebinding to the heme. The intensity ratio of the two modes remains constant for all data points, and thus we conclude that there is no interconversion between the two conformations at 293 K. The final spectrum at 15 ms demonstrates that there is no irreversible light-induced effect on the heme Fe.

The continuous variability in intensity of the CO modes associated with heme Fe over a 0.012−15 ms time scale is used to monitor and quantify ligand rebinding to heme Fe, and is depicted in Figures 4 and 5 for pH 5.6 and 8.5, respectively. The ΔA of the Fe^{2+}−CO bands shown in Figure 4A was measured as a function of time to determine the rate of recombination of CO to heme Fe at pH 5.6 ($k_{1945\ cm^{-1}} = 126 \pm 20\ s^{-1}$, $k_{1964\ cm^{-1}} = 122 \pm 20\ s^{-1}$) at room temperature (Figure 4B). The curves are three parameter fits to the experimental data according to first-order kinetics. The rate of recombination of CO to heme Fe ($k_{1945\ cm^{-1}} = 148 \pm 30\ s^{-1}$, $k_{1964\ cm^{-1}} = 158 \pm 32\ s^{-1}$) at pH 8.5 is depicted in Figure 5B.

Figure 6 collects TRS^2-FTIR difference spectra in the frequency range 1330−1550 cm^{-1}, where the 1387/1406 cm^{-1} ($\nu(COO^-)^{sym}$) of heme propionates, the peaks/troughs at 1465/1450 cm^{-1} ($\nu(COO^-)^{sym}$) of Glu, and the $\nu(COO^-)^{asym}$ of the heme propionate(s) at 1526 cm^{-1} have been observed at pH 5.6 and 8.5, respectively. The data suggest that, upon CO photolysis, the protein conformation changes near the heme Fe propionates and the distal Glu143 residue. The time evolution of the peaks/troughs depicted in Figure 6 demonstrate that these transient C−O stretches decay on a time scale coincident with the rebinding of CO to the heme Fe.

DISCUSSION

We report here the first detailed characterization and dynamics of the active site of OxdRE. We discuss our results with respect to (1) the presence of two distinct conformations of the catalytic center and (2) the effect of the protein residues on the bound CO ligand in order to counterbalance the back-donation from Fe(II) d_π electrons into the antibonding CO π^* orbitals. The ligand binding properties and the role of the protein environment that has been implicated in the catalytic properties of Oxd are important to exploit because the molecular mechanism by which the enzyme recognizes and converts aryl and alkyl aldoximes to their corresponding nitriles is largely unknown.

Origin of the CO-Binding Conformations. The interaction of CO with heme Fe(II) has been used to investigate the nature of the heme distal pocket in a number of heme-containing proteins and enzymes.[17,26−29] The electronic structure and/or the steric structure of the catalytic site (Figure 7) that is responsible for the unique Fe−C−O modes in Oxd may provide useful information on the catalytic mechanism of the enzyme. The insensitivity of the CO modes in OxdRE to pH indicates that

dx.doi.org/10.1021/jp205944e |J. Phys. Chem. B 2011, 115, 13012–13018

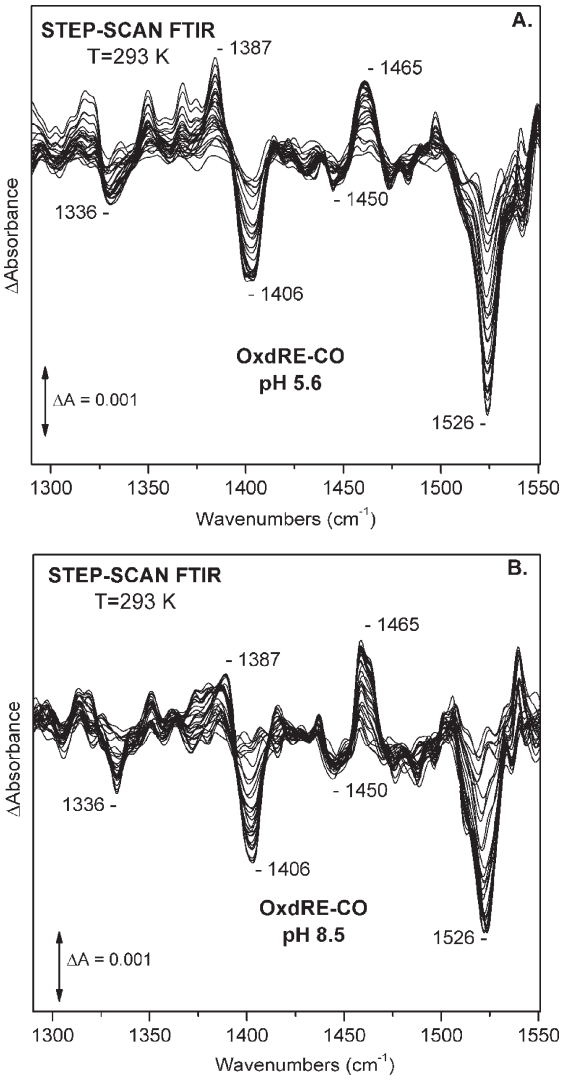

Figure 6. Time-resolved step-scan FTIR difference spectra of the OxdRE−CO adduct at pH 5.6 (A) and pH 8.5 (B) at 0.012, 0.037, 0.062, 0.125, 0.187, 0.250, 0.312, 0.375, 0.437, 0.500, 0.625, 0.750, 0.875, 1, 1.25, 1.5, 1.75, 2, 2.5, 3, 3.5, 4, 4.5, 5, 6, 7, 8, 9, 10, 11, 12, 13, and 15 ms subsequent to CO photolysis in the 1300−1550 cm^{-1} spectral range.

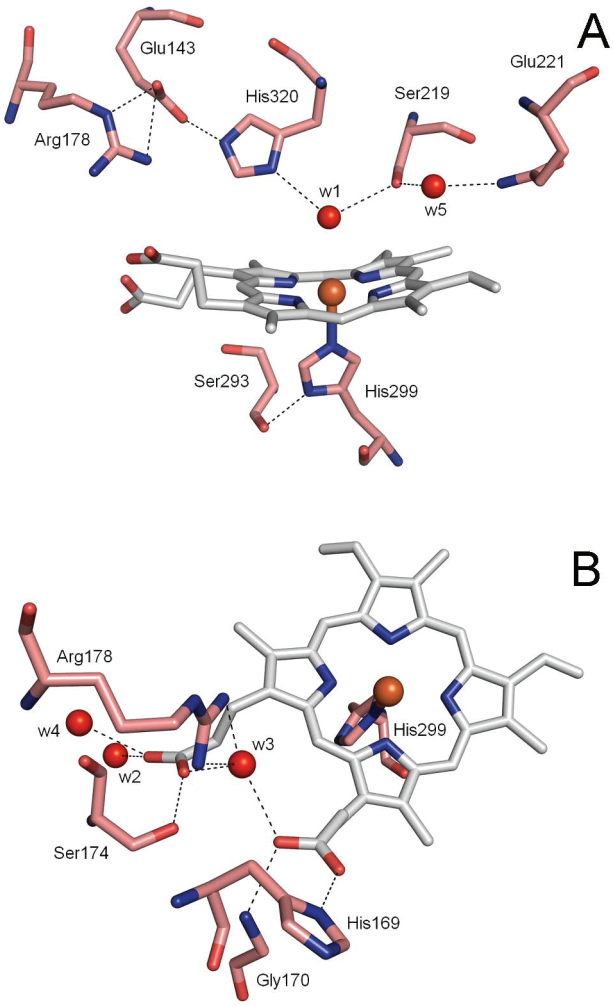

Figure 7. (A) Heme site of substrate-free OxdRE. (B) Hydrogen bonding network with the heme propionates. Water molecules are shown as red spheres. The dashed lines show the possible hydrogen bonds. PDB (Protein Data Bank) accession code 3A15.[11]

in the pH 5.6−8.5 range His320 and the distal residues are not directly involved in controlling the properties of the heme Fe bound CO. Alternatively, the pH insensitivity could indicate that distal residues that may interact with the bound CO do not undergo any structural or protonation changes in the pH 5.6−8.5 range; however, this would not be expected for His.

It is well-known from resonance Raman (RR) and computational studies that the properties of the trans ligand of carbonmonoxy−heme complexes can affect bonding between the iron and the distal CO and, thus, its vibrational frequency.[30−33] OxdA and OxdRE have a Fe−His stretching frequency of 226 cm^{-1}, which is indicative of a moderate to strong H-bond to the proximal ligand in comparison to no H-bond (ν(Fe−His) ∼ 200 cm^{-1}) and strong H-bond (ν(Fe−His) ∼ 240 cm^{-1}).[5,6,10] The crystal structure indicates that the proximal His299 is H-bonded to the carbonyl group of Ser293 (Figure 7).[11] The observed ν(Fe−CO) of OxdA at 512 cm^{-1} is higher than those of many other hemoproteins which have weaker Fe−His bonds, including myoglobin (ν(Fe−CO) = 507 cm^{-1}).[6,17] It was suggested that in Oxd there are positively charged or proton-donating residues in the distal pocket that affect the properties of the bound CO (Figure7).[6] Alternatively, it was proposed that the hydrogen bonding between the proximal His and Ser293 could be broken upon CO binding, leading to weakening of the Fe−His299 bond and the concomitant increase of the ν(Fe−CO) and decrease of the C−O frequencies, respectively.[6] In the absence of any observable effect from the His320 and Ser219 residues in the distal environment of the bound CO, we suggest that the properties of the proximal environment, the H-bond between the N_δ proton of the proximal His299 and backbone carbonyl oxygen from Ser293, and the heme propionates (see below) are responsible for the relatively high ν(Fe−CO) and the C−O frequencies. This explanation finds support from recent density functional theory (DFT) studies on axial and equatorial effects on heme−CO vibrational modes.[30] The computations revealed that the strength of the Fe−His bond depends on the H-bond status of the imidazole side chain and the weakening of this bond increases ν(CO) with little change in ν(Fe−CO), whereas the opposite pattern is predicted for tension generated by the protein environment. We suggest that it is unlikely that the strength of the

Fe−His bond alone contributes to the relatively high Fe−CO and C−O stretching frequencies in Oxd−CO. We propose that the neutralization of the negatively charged propionate groups, as indicated by the strong intensity at 1526 cm^{-1} ($\nu(COO^-)^{asym}$) in the CO photodissociation experiments, modulates the ν(Fe−CO)/ν(CO) back-bonding correlation in a manner similar to electron-withdrawing groups on porphines that alter the ν(CO) by up to 20 cm^{-1}.[30]

Relaxation Dynamics. The rate of CO recombination to OxdRE is slower than that observed for Mb, suggesting that the ligand escapes the distal site after dissociation from the heme, and protein fluctuations delay the rebinding process.[34,35] The changes caused by photolysis of the heme-bound CO ligand can be seen as troughs at 1945 and 1964 cm^{-1} in the TRS^2-FTIR and "light" minus "dark" difference FTIR spectra. Putative B-states of photodissociated CO ligands that are trapped inside the protein matrix typically display weak bands near 2130 cm^{-1}, providing evidence for the existence of ligand docking sites.[26,34−36] Accordingly, we assign the 2138 cm^{-1} mode we observe in the photolyzed OxdRE to a B state in which CO is funneled into a docking site. It is anticipated that OxdRE has preexisting cavities that are modestly perturbed by the photodissociated CO from the heme Fe. Protein fluctuations have been observed in heme proteins where the recombination of CO from the docking site to the heme is slowed substantially.[26,34−36] This way, the large scale protein fluctuations open exit channels through which ligands migrate into other internal cavities before they finally escape from the protein.

TRS^2-FTIR spectroscopy and the "light" minus "dark" FTIR approach have proven to be very powerful techniques in studying changes at the level of individual amino acids during protein action.[21−25,37,38] The intensity changes and frequency shifts of side chains and backbone structures observed in the TRS^2-FTIR and "light" minus "dark" difference FTIR spectra are the result of the perturbation induced by the photodissociated CO from the heme Fe. Based on the crystal structure of OxdRE the heme 6-propionate is directed to the proximal side, and its conformation is stabilized by interactions with two water molecules (w2 and w4) and the side chain of Ser174 (Figure 7). On the other hand, the 7-propionate is directed toward the distal side. A single water molecule (w3) is shared by the two propionates for hydrogen bonding. In the distal heme pocket, a hydrogen bond network exists among His320, Glu143, and Arg178. The following discussion for the behavior of the ring propionates and the water molecules is based on our tentative assignments. The observation of the negative peaks at 1696 and 1710 cm^{-1} may be attributed to deprotonation of the heme propionates upon CO photolysis. However, the concurrent presence of negative signals at 1526, 1568, and 1406 cm^{-1} that are attributed to the deprotonated propionates indicates that this is not the case. We suggest there is an equilibrium of $COO^- \leftrightarrow$ COOH. The lack of pH sensitivity between pH 5.6 and 8.5 indicates that the equilibrium of $COO^- \leftrightarrow$ COOH is not affected in that pH range. The reduced intensity and the shift of the 1526 cm^{-1} mode to 1523 cm^{-1}, and the concomitant increased intensity and shift of the 1568 cm^{-1} mode to 1562 cm^{-1} upon H/D exchange, indicate a dependence of heme propionates on local environment and/or hydrogen bonding interactions. To account for the lack of an observable negative peak at 1710 cm^{-1} in the D_2O experiments, we suggest that the change of the H-bonding connectivity in the local environment of heme propionates upon H/D exchanges also affects the protonated form, and thus we do not observe a negative peak upon the induced perturbation (CO photolysis from heme Fe). Therefore, the proton connectivity between the heme propionates and the nearby residues is altered in the presence of D_2O, allowing the heme propionates to adopt a conformation that is different from that observed in the pH experiments. The detection of the deprotonated propionate(s) is not only the result of the induced perturbation, but rather a combination of the H-bonded connectivity of the groups that is perturbed in the presence of D_2O. This sequential or concerted H-bonded connectivity between the environments sensed by the heme Fe propionates could have an activation energy for proton motion.[25] The first step in locating possible sites of proton motion requires identification of labile protons that could be perturbed by ligand motion, in this case, the CO photodissociation from heme Fe. On this line, the deprotonation of Glu143 which is H-bonded to His320 can initiate a cascade of events contributing to the reorganization of the OH group of the heme-bound substrate. The latter forms two hydrogen bonds with Ser219 and His 320. Our proposal of structural rearrangements in the proximal side finds support from the crystal structures, where it was reported that in the distal heme pocket the hydrogen-bond network was retained among Glu143, Arg178, and His320, as was the case of the substrate-free form. On the other hand, large conformational differences were observed at the proximal side of the heme.

The data reported here further support the involvement of the proximal His299 in a back-bonding influence other than the distal polarity. Another structural feature that modulates back-bonding, and is a determinant of the strength of the Fe−C and C−O bonds, is the neutralization of the negatively charged propionate groups on the heme that modulates the ν(Fe−CO)/ν(CO) back-bonding correlation in a manner similar to electron-withdrawing substituents on porphines.[30]

CONCLUSIONS

The vibrational properties of the CO adduct of OxdRE indicate the formation of a photolabile species in which the proximal histidine and the H-bonding interactions of the negatively charged heme propionates are dominant factors in controlling the strength of the Fe−CO bond. The latter observation indicates that other factors beyond the well-known proximal and distal back-bonding contributions are effective in Oxd. Taken together, the data presented here and those recently reported indicate that the distal residues control the proper orientation of the bound aldoxime and, thus, modulate the heme conformation from inactive to active.[11] Obviously, there is communication linkage between the distal and proximal sites through bond networks suggesting that there is a coupling between ligation dynamics and the environment sensed by the heme propionates. The complexity of the structural implications involved in the transition from oxidized to reduced state in the presence of aldoxime should serve as a basis for uncovering the dynamic processes involved in the reaction mechanism of the enzyme.

AUTHOR INFORMATION

Corresponding Author

*E-mail: effiep@ucy.ac.cy.

Present Addresses

[||]Department of Environmental Management, Cyprus University of Technology, P.O. Box 50329, 3603 Lemesos, Cyprus.

■ ACKNOWLEDGMENT

This work was partially supported by the University of Cyprus and Cyprus Research Promotion Foundation, Grant ANAVATH-MISI/PAGIO/0308/14 to E.P., and a Grant-in-Aid for Scientific Research (B) (19370059) from the Japan Society for the Promotion of Science to S.A.

■ ABBREVIATIONS USED

Oxd, aldoxime dehydratase; OxdRE, aldoxime dehydratase from *Rhodococcus* sp. N-771; OxdA, aldoxime dehydratase from *Pseudomonas chlororaphis* B23; TRS^2-FTIR, time-resolved step-scan Fourier transform infrared; RR, resonance Raman

■ REFERENCES

(1) Kobayashi, M.; Shimizu, S. *Nat. Biotechnol.* **1998**, *16*, 733–736.
(2) Kobayashi, M.; Shimizu, S. *Curr. Opin. Chem. Biol.* **2000**, *4*, 95–102.
(3) Kato, Y.; Ooi, R.; Asano, Y. *Appl. Environ. Microbiol.* **2000**, *66*, 2290–2296.
(4) Asano, Y. *J. Biotechnol.* **2002**, *94*, 65–72.
(5) Konishi, K.; Ishida, K.; Oinuma, K.-I.; Ohta, T.; Hashimoto, Y.; Higashibata, H.; Kitagawa, T.; Kobayashi, M. *J. Biol. Chem.* **2004**, *279*, 47619–47625.
(6) Oinuma, K.-I.; Ohta, T.; Konishi, K.; Hashimoto, Y.; Higashibata, H.; Kitagawa, T.; Kobayashi, M. *FEBS Lett.* **2004**, *568*, 44–48.
(7) Konishi, K.; Ohta, T.; Oinuma, K.-I.; Hashimoto, Y.; Kitagawa, T.; Kobayashi, M. *Proc. Natl. Acad. Sci. U.S.A.* **2006**, *103*, 564–568.
(8) Kobayashi, K.; Kubo, M.; Yoshioka, S.; Kitagawa, T.; Kato, Y.; Asano, Y.; Aono, S. *ChemBioChem* **2006**, *7*, 2004–2009.
(9) Kobayashi, K.; Yoshioka, S.; Kato, Y.; Asano, Y.; Aono, S. *J. Biol. Chem.* **2005**, *280*, 5486–5490.
(10) Kobayashi, K.; Biswajit, P.; Yoshioka, S.; Kato, Y.; Asano, Y.; Kitagawa, T.; Aono, S. *J. Inorg. Biochem.* **2006**, *100*, 1069–1074.
(11) Sawai, H.; Sugimoto, H.; Kato, Y.; Asano, Y.; Shiro, Y.; Aono, S. *J. Biol. Chem.* **2009**, *284*, 32089–32096.
(12) Pinakoulaki, E.; Ohta, T.; Soulimane, T.; Kitagawa, T.; Varotsis, C. *J. Biol. Chem.* **2004**, *279*, 22791–22794.
(13) Pinakoulaki, E.; Yoshimura, H.; Daskalakis, V.; Yoshioka, S.; Aono, S.; Varotsis, C. *Proc. Natl. Acad. Sci. U.S.A.* **2006**, *103*, 14796–14801.
(14) Ohta, T.; Pinakoulaki, E.; Soulimane, T.; Kitagawa, T.; Varotsis, C. *J. Phys. Chem. B* **2004**, *108*, 5489–5491.
(15) Pinakoulaki, E.; Yoshimura, H.; Yoshioka, S.; Aono, S.; Varotsis, C. *Biochemistry* **2006**, *45*, 7763–7766.
(16) Pinakoulaki, E.; Varotsis, C. *Biochemistry* **2003**, *42*, 14856–14861.
(17) Ray, G. B.; Li, X. Y.; Ibers, J. A.; Sessler, J. L.; Spiro, T. G. *J. Am. Chem. Soc.* **1994**, *116*, 162–176.
(18) Hellwig, P.; Behr, J.; Ostermeier, C.; Richter, O.-M. H.; Pfitzner, U.; Odenwald, A.; Ludwig, B.; Michel, H.; Mäntele, W. *Biochemistry* **1998**, *37*, 7390–7399.
(19) Hellwig, P.; Soulimane, T.; Buse, G.; Mäntele, W. *Biochemistry* **1999**, *38*, 9648–9658.
(20) Behr, J.; Hellwig, P.; Mäntele, W.; Michel, H. *Biochemistry* **1998**, *37*, 7400–7406.
(21) Rich, P. R.; Breton, J. *Biochemistry* **2001**, *40*, 6441–6449.
(22) Ingledew, W. J.; Smith, S. M. E.; Salerno, J. C.; Rich, P. R. *Biochemistry* **2002**, *41*, 8377–8384.
(23) Bailey, J. A.; Tomson, F. L.; Mecklenburg, S. L.; MacDonald, G. M.; Katsonouri, A.; Puustinen, A.; Gennis, R. B.; Woodruff, W. H.; Dyer, R. B. *Biochemistry* **2002**, *41*, 2675–2683.
(24) Heitbrink, D.; Sigurdson, H.; Bolwien, C.; Brzezinski, P.; Heberle, H. *Biophys. J.* **2002**, *82*, 1–10.
(25) Koutsoupakis, C.; Soulimane, T.; Varotsis, C. *Biophys. J.* **2004**, *86*, 2438–2444.
(26) Nienhaus, K.; Deng, P.; Olson, J. S.; Warren, J. J.; Nienhaus, G. U. *J. Biol. Chem.* **2003**, *278*, 42532–42544.
(27) Shimada, H.; Caughey, W. S. *J. Biol. Chem.* **1982**, *257*, 11893–1190.
(28) Ramsden, J.; Spiro, T. G. *Biochemistry* **1989**, *28*, 3125–3128.
(29) Sage, T.; Morikis, D.; Champion, P. M. *Biochemistry* **1991**, *30*, 1227–1237.
(30) Xu, C.; Ibrahim, M.; Spiro, T. G. *Biochemistry* **2008**, *47*, 2379–2387.
(31) Li, X. Y.; Spiro, T. G. *J. Am. Chem. Soc.* **1988**, *110*, 6024–6033.
(32) Spiro, T. G.; Wasbotten, I. H. *J. Inorg. Biochem.* **2005**, *99*, 34–44.
(33) Varotsis, C.; Vamvouka, M. *J. Phys. Chem. B* **1998**, *102*, 7670–7673.
(34) Ostermann, A.; Waschipky, R.; Parak, F. G.; Nienhaus, G. U. *Nature* **2000**, *404*, 205–208.
(35) Schleerger, M.; Wagner, C.; Vellekoop, M. J.; Lendl, B.; Heberle, H. *Anal. Bioanal. Chem.* **2009**, *394*, 1869–1877.
(36) Koutsoupakis, C.; Soulimane, T.; Varotsis, C. *J. Am. Chem. Soc.* **2003**, *125*, 14728–14732.
(37) Koutsoupakis, C.; Pinakoulaki, E.; Stavrakis, S.; Daskalakis, V.; Varotsis, C. *Biochim. Biophys. Acta* **2004**, *1655*, 347–352.
(38) Kotting, C.; Gerwert, K. *ChemPhysChem* **2005**, *6*, 881–888.